

Photonic realization of the relativistic Dirac oscillator

S. Longhi

Dipartimento di Fisica, Politecnico di Milano, Piazza L. da Vinci 32, I-20133

Milano, Italy

A photonic realization of the Dirac oscillator (DO), i.e. of the relativistic extension of the quantum harmonic oscillator, is proposed for light propagation in fiber Bragg gratings. Transmission spectra clearly show the existence of electron and positron bound states of the DO, corresponding to resonance modes above and below the Bragg frequency, as well as the asymmetry of the energy spectrum for electron and positron branches. © 2022 Optical Society of America

OCIS codes: 000.2658,060.3735

The relativistic extension of the quantum harmonic oscillator, the so-called Dirac oscillator (DO) [1–3], provides a paradigmatic and exactly solvable model of relativistic quantum mechanics. Originally proposed in quantum chromodynamics in connection to quark confinement models in mesons and baryons [4], the DO has received great interest in relativistic many-body theories and supersymmetric relativistic quantum

mechanics (see [2, 3, 5–7] and references therein). The DO model is obtained from the free Dirac equation by the introduction of the external potential via a non-minimal coupling [1, 3, 7]. Since the resulting equation is linear in both momentum and position operators, in the nonrelativistic limit a Schrödinger equation with a quadratic potential is then obtained. In spite of the great amount of theoretical studies, the DO model in relativistic quantum mechanics and particle physics remains far from any experimental consideration. Recently, an increasing interest has been devoted to the investigation of quantum or classical systems capable of providing an accessible laboratory tool to test some peculiar phenomena rooted in the Dirac equation, such as Klein tunneling and Zitterbewegung [8]. Quantum and classical analogs of such two phenomena have been investigated in graphene, trapped ions, photonic crystals and metamaterials (see, e.g., [9–15] and references therein), with the first experimental observations of Klein tunneling and Zitterbewegung reported in Refs. [9–11]. Such experiments motivate the search for experimental systems that could simulate a relativistic DO. Recently, interesting insightful connections between the relativistic DO and the Jaynes-Cummings model of quantum optics have been pointed [16–18], and an experimental proposal of a two-dimensional DO using a single trapped ion has been presented [17].

It is the aim of this Letter to propose a classic wave optics analogue of the one-dimensional relativistic Dirac oscillator based on light propagation in engineered fiber Bragg gratings (FBGs). Let us consider light propagation in a FBG [19] with

a longitudinal refractive index $n(z) = n_0 + \Delta n h(z) \cos[2\pi z/\Lambda + \phi(z)]$, where n_0 is the effective mode index in absence of the grating, $\Delta n \ll n_0$ is a reference value of the index change of the grating, Λ is the nominal grating period defining the Bragg frequency $\omega_B = \pi c/(\Lambda n_0)$, c is the speed of light in vacuum, and $h(z)$, $\phi(z)$ describe the amplitude and phase profiles, respectively, of the grating. To study Bragg scattering of counterpropagating waves at frequencies close to ω_B , let $E(z, t) = \{u(z, t) \exp(-i\omega_B t + 2\pi i z n_0/\lambda_0) + v(z, t) \exp(-i\omega_B t - 2\pi i z n_0/\lambda_0) + c.c.\}$ be the electric field in the fiber, where $\lambda_0 = 2n_0\Lambda$ is the Bragg wavelength. The envelopes u and v of counterpropagating waves [see Fig.1(a)] satisfy the coupled-mode equations [19, 20]

$$[\partial_z + (1/v_g)\partial_t] u = iq(z)v \quad (1)$$

$$[\partial_z - (1/v_g)\partial_t] v = -iq^*(z)u \quad (2)$$

where $q(z) = (\pi\Delta n/\lambda_0)h(z) \exp[i\phi(z)]$ is the complex scattering potential and $v_g \sim c/n_0$ is the group velocity at the Bragg frequency. To highlight the analogy between light propagation in a FBG with suitable amplitude and and phase profiles, and the one-dimensional relativistic DO, let us introduce the dimensionless variables $x = z/Z$ and $\tau = t/T$, with characteristic spatial and time scales $Z = \lambda_0/(\pi\Delta n)$ and $T = Z/v_g$, and the new envelopes $\psi_{1,2}(z) = [u(z) \mp v(z)]/\sqrt{2}$. In this way, Eqs.(1-2) can be cast in the Dirac form

$$i\partial_\tau \psi = \sigma_x \{p_x - if(x)\sigma_z\} \psi + \sigma_z m(x)\psi \quad (3)$$

for the spinor wave function $\psi = (\psi_1, \psi_2)^T$, where σ_x and σ_z are the Pauli matrices, defined by

$$\sigma_x = \begin{pmatrix} 0 & 1 \\ 1 & 0 \end{pmatrix}, \quad \sigma_z = \begin{pmatrix} 1 & 0 \\ 0 & -1 \end{pmatrix}, \quad (4)$$

$p_x = -i(d/dx)$, and where we have set

$$m(x) = h(x) \cos[\phi(x)], \quad f(x) = -h(x) \sin[\phi(x)]. \quad (5)$$

In its present form, Eq.(3) is analogous to the one-dimensional Dirac equation [8], written in atomic units ($\hbar = c = 1$), with a space dependence mass m and with the momentum operator p_x substituted with $p_x - if(x)\sigma_z$. The space dependence of the particle mass m is known to describe the particle interaction with a scalar Lorentz potential, whereas the substitution $p_x \rightarrow p_x - if(x)\sigma_z$ corresponds to a non-minimal coupling which is essential to describe the relativistic DO (see, for instance, [7]). To realize the one-dimensional analog of the DO, let us choose the amplitude h and phase ϕ profiles of the grating such that $h \cos \phi = m_0$ and $h \sin \phi = -f(x) = \omega_s m_0 x$, i.e. (see Fig.1)

$$h(x) = m_0 \sqrt{1 + (\omega_s x)^2}, \quad \phi(x) = \text{atan}(\omega_s x), \quad (6)$$

where m_0 and ω_s are two arbitrary constants, corresponding to the particle rest mass and oscillation frequency of the DO in the non-relativistic limit [7]. Analytical expressions of the energy spectrum for the one-dimensional DO and of corresponding bound states can be derived following a standard procedure detailed e.g. in Ref. [7]. Let us

search for a solution to Eq.(3) of the form $\psi(x, \tau) = (\psi_+(x), \psi_-(x))^T \exp(-i\delta\tau)$, where δ is the energy eigenvalue of the Dirac Hamiltonian and $m(x)$, $f(x)$ are defined according to Eqs.(5) and (6). The functions ψ_+ and ψ_- are then found to satisfy the harmonic oscillator equation

$$-\frac{1}{2m_0} \frac{d^2\psi_{\pm}}{dx^2} + \frac{1}{2}m_0\omega_s^2 x^2 \psi_{\pm} = \frac{\delta^2 - m_0^2 \mp m_0\omega_s}{2m_0} \psi_{\pm}. \quad (7)$$

The eigenvalues of Eq.(7) are those of the non-relativistic harmonic oscillator. Assuming for the sake of definiteness $\omega_s > 0$, the positive-energy spectrum (electron branch) of the DO is thus given by

$$\delta_n = \sqrt{m_0^2 + 2m_0\omega_s(1+n)}, \quad n = 0, 1, 2, 3, \dots \quad (8)$$

whereas the negative-energy spectrum (positron branch) is given by

$$\delta_n = -\sqrt{m_0^2 + 2m_0\omega_s n}, \quad n = 0, 1, 2, 3, \dots \quad (9)$$

The corresponding eigenfunctions $\psi_{\pm}(x)$ can be simply expressed in terms of Hermite polynomials multiplied by a Gaussian function. It is worth pointing out two important properties of the spectrum of the one-dimensional DO. First, the non-relativistic limit of the DO is attained by considering the positive-energy branch of the spectrum in the limit $\omega_s/m_0 \rightarrow 0$; in this limit, from Eq.(8) one obtains at leading order $\delta_n = m_0 + \omega_s(1/2 + n) + (\omega_s/2)$ ($n = 0, 1, 2, 3, \dots$). The first two terms appearing in this expression of the energy have a simple physical meaning: m_0 is the rest energy of the particle whereas $\omega_s(1/2 + n)$ are the usual quantized energy levels

of the non-relativistic harmonic oscillator (please note that we used atomic units, i.e. $\hbar = c = 1$). The third term ($\omega_s/2$) is responsible for an additional energy shift of the zero-point energy, which is a characteristic feature of the DO (also found in the three-dimensional DO; see for instance [3, 5]). A second property of the DO, which readily follows from an inspection of Eqs.(8) and (9), is that the negative (positron) energy spectrum is not obtained from the positive (electron) energy spectrum by sign reversal ($\delta \rightarrow -\delta$), the positron branch possessing an additional bound state with energy $\delta = -m_0$. In our FBG realization of the DO, bound-states with positive and negative energies should correspond to trapped light states in the FBG with resonance frequencies above ($\delta > 0$) and below ($\delta < 0$) the Bragg frequency ω_B , respectively. In a FBG of finite length, the ideal amplitude profile $h(x)$, defined by Eq.(6), must be truncated, i.e. one has $h(x) = 0$ for $|x| > L/(2Z)$, where L is the grating length (see Fig.1). The effect of grating truncation is twofold. First, the bound states of the DO become actually resonance modes with a finite lifetime, which should be thus observable as narrow transmission peaks embedded in the stop band of the grating (see Fig.2 to be commented below). Second, the number of resonance modes sustained by the grating is finite owing to grating truncation. As an example, Fig.2(a) shows a typical transmission spectrum [power transmission versus normalized frequency detuning $\delta = (\omega - \omega_B)T$], as obtained by standard transfer matrix methods [19], of a FBG with length $L/Z = 10$ for parameter values $m_0 = 1$ and $\omega_s = 0.5$. Figure 2(b) shows the corresponding reflection-band diagram (dashed

area) of the grating in the (x, δ) plane [20], together with the electron ($\delta > 0$) and positron ($\delta < 0$) levels of the DO, as predicted by Eqs.(8) and (9); a snapshot of normalized intensity profiles $|\psi_+|^2 + |\psi_-|^2 = |u|^2 + |v|^2$ for a few low-order DO bound states are also depicted. According to Ref. [20], the band reflection diagram shows the local stop band of the grating, as a function of position x , which is determined by the inequality $|\delta - (1/2)(d\phi/dx)| < |h(x)|$. Note that the transmission peaks in Fig.2(a), embedded in the stop band of the FBG, occur precisely at the values δ_n predicted by Eqs.(8) and (9). Note also the asymmetry of the transmission spectrum around $\delta = 0$, with an additional resonance in the positron ($\delta < 0$) branch of the spectrum with no counterpart in the electron ($\delta > 0$) branch. According to the band reflection diagram of Fig.2(b), the number of bound states of the DO sustained by the truncated FBG are about 6 in each branch. For the sake of clearness, only 3 modes in the electronic branch, and 4 modes in the positron branch, are depicted in the figure. Note that, as expected, the resonance widths increase for higher-order modes (i.e. for increasing quantum number n) because of the narrowing of the gap regions that sustain light trapping for such modes. Note also that additional oscillations in the transmission spectrum, outside the stop band of the grating, are clearly visible in Fig.2(a). However, such oscillations do not correspond to resonance states of the DO, rather they arise because of an impedance mismatch between the grating ($|z| < L/2$) and non-grating ($|z| > L/2$) regions of the fiber, like in an ordinary non-apodized FBG (see, for instance, [19]). In physical units, for typical

parameter values $n_0 = 1.45$, $\Delta n = 1 \times 10^{-4}$ and $\lambda_0 = 1560$ nm which apply to FBGs used in optical communications, the spatial (Z) and temporal (T) scales for the example in Fig.2 are $Z \simeq 5$ mm and $T \simeq 24$ ps, respectively. Hence, in physical units the grating length is $L \simeq 5$ cm, the unit scale of (non-angular) frequency detuning in Fig.2 is $1/(2\pi T) \simeq 6.6$ GHz, and the maximum index change requested to realize the FBG, reached at the FBG edges $z = \pm L/2$, is $\Delta n \sqrt{1 + (\omega_s L/2Z)^2} \simeq 2.69 \times 10^{-4}$. Such a nonuniform FBG should be easily manufactured with currently available FBG technology based on UV continuous laser writing [21]. According to Fig.2(a) and following the previous discussion, in an experiment the resonant states of the DO could be simply detected from spectrally-resolved transmission measurements. Like in any FBG structure supporting trapped modes (e.g. Fabry-Perot or phase-shifted FBGs), the transmission peaks of high-Q resonant modes may be strongly reduced by unavoidable intrinsic losses in the FBG (see, for instance, [22]). As an example, Fig.2(c) shows the transmission spectrum of the FBG of Fig.2(a), but assuming a power loss rate $\alpha = 0.5$ m⁻¹ in the fiber (value taken from Ref. [22]). Note that, in spite of the great peak reduction, the resonant states as well as the asymmetry of the spectrum are still clearly visible.

In conclusion, a photonic realization of a Dirac oscillator, based on light propagation in FBGs, has been proposed. Electron and positron bound states of the DO should be clearly visible in spectrally-resolved transmission measurements as resonances above and below the Bragg frequency.

The author acknowledges support by the Italian MIUR (PRIN 2008 project "Analogie ottico-quantistiche in strutture fotoniche a guida donda").

Author E-mail address: longhi@fisi.polimi.it

References

1. M. Moshinsky and A. Szczepaniak, "The Dirac oscillator", J. Phys. A **22**, L817 (1989).
2. M. Moshinsky and Y.F. Smirnov, *The Harmonic Oscillator in Modern Physics* (Harwood, Amsterdam, 1996).
3. R.P. Martinez-y-Romero, H.N. Nunez-Yepez, and A.L. Salas-Brito, "Relativistic quantum mechanics of a Dirac oscillator", Eur. J. Phys. **16**, 135 (1995).
4. D. Ito, K. Mori, and E. Carrieri, "An example of Dynamical Systems with Linear Trajectory" Nuovo Cimento **51A**, 1119 (1967).
5. J. Bentez, R.P. Martnez-y-Romero, H.N. Nuez-Yepez, and A.L. Salas-Brito, "Solution and hidden supersymmetry of a Dirac oscillator", Phys. Rev. Lett. **64**, 1643 (1990); see also: *Erratum*, Phys. Rev. Lett. **65**, 2085 (1990).
6. R.P. Martriaanez-y-Romero, M. Moreno, and A. Zentella, "Supersymmetric properties and stability of the Dirac sea", Phys. Rev. D **43**, 2036 (1991).
7. F. Dominguez-Adame and M. A. Gonzalez , "Solvable Linear Potentials in the Dirac Equation", Europhys. Lett. **13**, 193 (1990).

8. W. Greiner, *Relativistic Quantum Mechanics* (Springer-Verlag, Berlin, 1990).
9. A.F. Young and P. Kim, "Quantum interference and Klein tunnelling in graphene heterojunctions", *Nature Phys.* **5**, 222 (2009).
10. N. Stander, B. Huard, and D. Goldhaber-Gordon, "Evidence for Klein Tunneling in Graphene p-n Junctions", *Phys. Rev. Lett.* **102**, 026807 (2009).
11. R. Gerritsma , G. Kirchmair, F.Zähringer, E. Solano, R. Blatt, and C.F. Roos, "Quantum simulation of the Dirac equation", *Nature* **463**, 68 (2010).
12. R.A. Sepkhanov, Ya. B. Bazaliy, and C.W.J. Beenakker, "Extremal transmission at the Dirac point of a photonic band structure", *Phys. Rev. A* **75**, 063813 (2007).
13. O. Peleg, G. Bartal, B. Freedman, O. Manela, M. Segev, and D.N. Christodoulides, "Conical Diffraction and Gap Solitons in Honeycomb Photonic Lattices", *Phys. Rev. Lett.* **98**, 103901 (2007).
14. X. Zhang, "Observing Zitterbewegung for Photons near the Dirac Point of a Two-Dimensional Photonic Crystal", *Phys. Rev. Lett.* **100**, 113903 (2008).
15. L.-G. Wang, Z.-G. Wang, and S.-Y. Zhu, "Zitterbewegung of optical pulses near the Dirac point inside a negative-zero-positive index metamaterial", *EPL* **86**, 47008 (2009).
16. P. Rozmej and R. Arvieu, "The Dirac Oscillator. A relativistic version of the Jaynes-Cummings model", *J. Phys. A* **32**, 5367 (1999).
17. A. Bermudez, M.A. Martin-Delgado, and E. Solano, "Exact mapping of the 2+1

Dirac oscillator onto the Jaynes-Cummings model: Ion-trap experimental proposal”, Phys. Rev. A **76**, 041801(R) (2007).

18. A. Bermudez, M.A. Martin-Delgado, and A. Luis, ”Nonrelativistic limit in the 2+1 Dirac oscillator: A Ramsey-interferometry effect”, Phys. Rev. A **77**, 033832 (2008).
19. T. Erdogan, ”Fiber Grating Spectra”, J. Lightwave Technol. **15**, 1277 (1997).
20. L. Poladian, ”Graphical and WKB analysis of nonuniform Bragg gratings”, Phys. Rev. E **48**, 4758 (1993).
21. A. Asseh, H. Storoy, B. Sahlgren, and R. Stubbe, ”A writing technique for long fiber Bragg gratings with complex reflectivity profiles”, J. Lightwave Technol. **15**, 1419 (1997).
22. Y. Liu, L. Wei, and J.W.Y. Lit, ”Transmission loss of phase-shifted fiber Bragg gratings in lossy materials: a theoretical and experimental investigation”, Appl. Opt. **46**, 6770 (2007).

List of Figure Captions.

Fig.1. (a) Schematic of a FBG. (b) and (c) Example of FBG amplitude and phase profiles that realize the analog of the Dirac oscillator ($m_0 = 1$, $\omega_s = 0.5$, $L/Z = 10$).

Fig.2. (Color online) (a) Numerically-computed power transmission (dB units) of a lossless FBG with amplitude and phase profiles shown in Fig.1, and (b) corresponding reflection band diagram (dashed area). In (b) a few low-order intensity profiles of trapped modes in the electron and positron branches are also depicted. (c) Same as (a), but for a lossy FBG (power loss rate $\alpha = 0.05 \text{ m}^{-1}$).

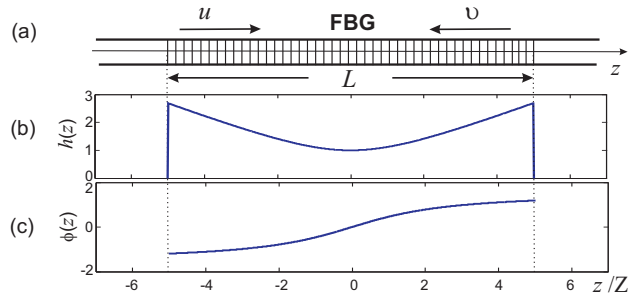


Fig. 1. (a) Schematic of a FBG. (b) and (c) Example of FBG amplitude and phase profiles that realize the analog of the Dirac oscillator ($m_0 = 1$, $\omega_s = 0.5$, $L/Z = 10$).

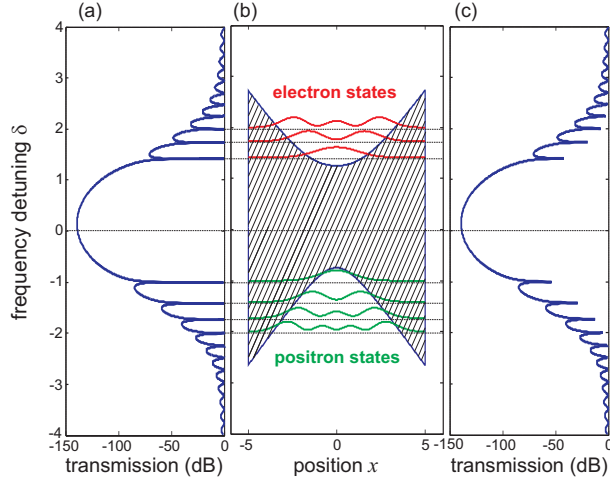


Fig. 2. (Color online) (a) Numerically-computed power transmission (dB units) of a lossless FBG with amplitude and phase profiles shown in Fig.1, and (b) corresponding reflection band diagram (dashed area). In (b) a few low-order intensity profiles of trapped modes in the electron and positron branches are also depicted. (c) Same as (a), but for a lossy FBG (power loss rate $\alpha = 0.05 \text{ m}^{-1}$).